JOURNAL OF MAGNETIC RESONANCE **130,** 321–328 (1998)
ARTICLE NO. MN971326

Magnetization Transfer Imaging of Rat Brain under Non-steady-state Conditions. Contrast Prediction Using a Binary Spin–Bath Model and a Super-Lorentzian Lineshape[1]

Bruno Quesson, Eric Thiaudière, Christophe Delalande, Jean-Francois Chateil, Chrit T. W. Moonen, and Paul Canioni

Résonance Magnétique des Systèmes Biologiques, UMR 5536, C.N.R.S.-Université Victor Segalen Bordeaux 2, Bordeaux, France

Received July 22, 1997

Magnetization transfer contrast imaging using turbo spin echo and continuous wave off-resonance irradiation was carried out on rat brain *in vivo* at 4.7 T. By systematically varying the off-resonance irradiation power and the offset-frequency, the signal intensities obtained under steady-state for both transverse and longitudinal magnetization were successfully analyzed with a simple binary spin–bath model taking into account a free water compartment and a pool of protons with restricted motions bearing a super-Lorentzian lineshape. Due to important RF power deposition, such experimental conditions are not practical for routine imaging on humans. An extension of the model was derived to describe the system for shorter off-resonance pulse duration, i.e., when the longitudinal magnetization of the free protons has not reached a steady-state. Data sets obtained for three regions of interest, namely the *corpus callosum,* the basal ganglia, and the temporal lobe, were correctly interpreted for off-resonance pulse durations varying from 0.3 to 3 s. The parameter sets obtained from the calculations made it possible to predict the contrast between the different regions as a function of the pulse power, the offset frequency, and pulse duration. Such an approach could be extended to contrast prediction for human brain at 1.5 T.

Key Words: **magnetization transfer imaging; rat brain; fast imaging; transient decay.**

INTRODUCTION

Magnetization transfer (MT) imaging is nowadays widely applied to clinical investigations of CNS diseases such as multiple sclerosis (*1, 2*), optic neuritis (*3*), experimental Wallerian degeneration (*4*), and experimental toxic demyelination (*5*). This technique has been shown to improve contrast (*4, 6*), and the tissue dependence of magnetization exchange has already been demonstrated (*7–9*). Moreover, MT contrasts provide additional information on the composition of tissues, which cannot be derived from conventional imaging based on relaxation behavior of the spins. The principle of MT imaging is based on the interaction between mobile protons of ''free'' water (pool A) and protons with restricted motions (pool B) in macromolecules and lipid bilayers (*10*). In the presence of such an interaction, a selective irradiation of the ''immobile'' proton pool, at an offset frequency of several kilohertz with respect to the water resonance, will cause a partial saturation of the former and a decrease in the intensity of the latter, thus creating contrast (*11*). The observed MT contrast can be modulated according to experimental constraints, which are the offset frequency of the MT pulse along with its amplitude, duration, and shape.

In clinical imaging, MT contrast is generated by many different acquisition protocols. Short (several milliseconds) (*1, 5, 12–14*) or long pulses (several hundreds of milliseconds) (*9*) are used for irradiating the ''immobilized'' protons. Considering the apparent T_1 values of free water pool in the human at 0.5–2 T, its longitudinal magnetization is clearly not under steady-state. Thus it seems difficult to derive the relaxation parameters and the rate constant of exchange between the two pools from such protocols. Nevertheless, such knowledge is essential to predict the behavior of the system, and then to estimate the optimal conditions for contrast.

To account for the observed MT contrast, the simplest model by far is the binary spin–bath model (BSBM), first proposed by Edzes and Samulski (*10*). A more advanced model was proposed which took into account the direct effect of the off-resonance pulse on the longitudinal magnetization of free water. Caines *et al.* (*15*), Wu (*16*), and Henkelman *et al.* (*17*) derived similar expressions for longitudinal magnetization of pool A, as a function of the irradiation frequency and the amplitude of the MT pulse, under steady-state saturation.

In order to derive the relaxation parameter from such a model, it is required to investigate the system under a number of experimental conditions, namely MT pulse power and offset frequency. Moreover, Henkelman's model was more adequate to fit experimental data by using a super-Lorentzian lineshape for the immobilized protons. Such a study has been conducted successfully in our laboratory on the rat brain *in vivo* at 4.7 T (*18*). Other interesting approaches have been proposed by Adler, Swanson, and Yeung (*19–22*). The purpose of those studies was to solve the equations governing

[1] This work was supported by grants from the Conseil Régional d'Aquitaine, the Association pour la Recherche contre le Cancer, and Bruker Spectrospin SA.

1090-7807/98 $25.00

the transient response of heterogeneous spin systems. Several methods were investigated, based on the use of the Laplace transform of Bloch's equations (*19*), on the projection operators (*20*), or on the reformulation of spin–bath model equations by the Redfield–Provotorov theory (*21*). Moreover, the same authors proposed a more complicated model with three components (*22*). In another very recent work (*23*), Listerud used the fixed point lemma technique to solve the Bloch equations in the transient decay. He supposed a Lorentzian lineshape for both pools A and B, but no experimental data sets were analyzed according to the solution presented.

The purpose of this work was to model MT signals obtained at 4.7 T with a fast imaging RARE sequence under transient decay of magnetization. Signal intensities from the *corpus callosum,* the basal ganglia, and the temporal lobe of the healthy rat brain *in vivo* were analyzed using a modified two-pool system derived from Henkelman's model which was previously found to fit correctly the MT data obtained *ex vivo* (*17*) and *in vivo* (*18*). The relaxation parameters obtained from the fits allowed the prediction of contrast as a function of the irradiation power, duration, and offset frequency of the MT pulse. Thus, the acquisition conditions leading to optimal contrast values between the considered regions were calculated. This approach was applied to tumoral regions of the rat brain at 4.7 T and to human brain at 1.5 T.

THEORETICAL BACKGROUND

The two-pool system studied in the present work is composed of a liquid pool (conventionally called A) and a semi-solid pool (called B), both having an independent longitudinal relaxation rate ($R_A = 1/T_{1A}$, $R_B = 1/T_{1B}$). M_O^A and M_O^B are the number of spins of pools A and B, respectively. Conventionally, M_O^A is normalized to 1. The magnetization transfer rate between the two pools is characterized by a fundamental rate constant R. In fact, as previously discussed by Henkelman *et al.* (*17*), the rate of exchange is $RM_O^B M_O^A$ in either direction between the two pools. With this notation, the Bloch equations can be written to include the effect of a continuous wave irradiation of amplitude ω_1 applied at an offset frequency Δ

$$\frac{dM_z^{A,B}}{dt} = R_{A,B}(M_O^{A,B} - M_z^{A,B}) - RM_O^{B,A}M_z^{A,B} + RM_O^{A,B}M_z^{B,A} + \omega_1 M_y^{A,B} \quad [1],[2]$$

$$\frac{dM_x^{A,B}}{dt} = -\frac{M_x^{A,B}}{T_{2A,B}} - 2\pi\Delta^{A,B}M_y^{A,B} \quad [3],[4]$$

$$\frac{dM_y^{A,B}}{dt} = -\frac{M_y^{A,B}}{T_{2A,B}} + 2\pi\Delta^{A,B}M_x^{A,B} - \omega_1 M_z^{A,B}, \quad [5],[6]$$

where $M_z^{A,B}$, $M_x^{A,B}$, $M_y^{A,B}$ are the longitudinal and transverse magnetizations of pool A or B, respectively. In order to simplify the solution of Eqs. [1]–[6], the analysis of the MT mechanism has previously been achieved under steady-state saturation ($dM/dt = 0$), requiring an irradiation pulse length of several seconds. It has been demonstrated that the two-pool model was successful under such experimental conditions to account for the observed signals on several tissue models.

In the present study, the same approach as that of Henkelman's group is followed to describe signal evolution before a steady-state has been reached. Therefore, under the condition that the transverse magnetization has reached a steady-state during off-resonance RF irradiation, a simplification of Eqs. [3] and [4] is reached:

$$M_y^{A,B} = \frac{-M_x^{A,B}}{2\pi\Delta^{A,B}T_{2A,B}} = \frac{-\omega_1 T_{2A,B}}{1 + (2\pi\Delta^{A,B}T_{2A,B})^2} M_z^{A,B}. \quad [7]$$

We define a parameter R_{rfi} representing the rate at which longitudinal magnetization is lost

$$R_{rf(A,B)} = \frac{\omega_1^2 T_{2A,B}}{1 + (2\pi\Delta^{A,B}T_{2A,B})^2}, \quad [8]$$

which can be written in a more formal way as

$$R_{rfi}(2\pi\Delta) = \omega_i^2 \pi g_i(2\pi\Delta), \quad [9]$$

where $g_i(2\pi\Delta)$ is the absorption lineshape for the pool i. As pointed out in several papers, the lineshape of protons with restricted motion $g_B(2\pi\Delta)$ does not seem to be Lorentzian. Gaussian and super-Lorentzian functions were suggested to improve the fit of data acquired from a wide scale of irradiation amplitude and offset-frequency, because such lineshapes are expected to arise from partially ordered materials. For conciseness, we do not report the mathematical expressions of these lineshapes, which can be found in Ref. (*24*).

The differential equations for longitudinal magnetization of pool A and B can be modified to introduce R_{rfi} as a parameter

$$\frac{dM_z^{A,B}}{dt} = \alpha_{A,B}M_z^{A,B} + R_{A,B}M_O^{A,B} + RM_O^{A,B}M_z^{B,A} \quad [10],[11]$$

where

$$\alpha_{A,B} = -(R_{A,B} + RM_O^{B,A} + R_{rf(A,B)}). \quad [12],[13]$$

The behavior of longitudinal magnetization is bi-exponential for both pool A and B. The solution for pool A (and B) is a function of Δ and ω_1 and has the expression

$$M_z^A(t) = c_1\exp(m_1 t) + c_2\exp(m_2 t) + \frac{RR_B M_O^B - \alpha_B R_A}{m_1 m_2} \quad [14]$$

$$m_{1,2} = \frac{\alpha_A + \alpha_B \pm \sqrt{(\alpha_A - \alpha_B)^2 + 4R^2M_O^B}}{2}. \quad [15]$$

For long pulse duration as compared to $(m_{1,2})^{-1}$, M_z^A reaches a steady-state called M_{ss}^A, corresponding to the third term of Eq. [14]. M_{ss}^A has the same expression as that reported in Henkelman's study (Eq. [9] of (*17*)) as well as in Caines *et al.* (*15*) and Wu (*16*). c_1 and c_2 are constants determined experimentally and $m_{1,2}$ represent the longitudinal relaxation rates of pool A ($1/T_{1sat}$) under saturation of pool B. From Eqs. [14] and [15], it appears that m_1 and m_2 are strictly negative and $m_2 < m_1$. If m_2/m_1 is high enough and c_2/c_1 approaches zero, as it will be shown below, it is possible to assume that the second term in the relaxation process of Eq. [14] becomes negligible. Longitudinal magnetization of pool A is simplified to a monoexponential decay:

$$\begin{aligned} M_z^A(t) &= c_1\exp(m_1t) + \frac{RR_BM_O^B - \alpha_BR_A}{m_1m_2} \\ &= (M_O^A - M_{ss}^A)\exp(m_1t) + M_{ss}^A. \end{aligned} \quad [16]$$

From this final equation and the expressions of M_{ss}^A and m_1, it appears that the determination of the six parameters R_A, R_B, R, M_O^B, T_{2A}, T_{2B} is necessary to fully describe the transient decay of observed signals under irradiation of pool B. Unfortunately, Henkelman's model was written as a function of five independent parameters, namely R, R_B, RM_O^B/R_A, $1/R_AT_{2A}$, T_{2A}, T_{2B}. Moreover, as has been observed by Caines *et al.* (*15*), unique sets of the six parameters mentioned above cannot be obtained by fitting M_{ss}^A in Eq. [16] to experimental data because steady-state measurements do not contain explicit reference to absolute time scale.

This problem can be circumvented by estimating R_A from inversion-recovery experiments. A simple relation between R_A and R_A^{obs} can be extracted from Eq. [15], setting ω_1 equal to zero (i.e., $R_{rfA} = R_{rfB} = 0$),

$$R_A = \frac{R_A^{obs}}{1 + \dfrac{RM_O^B(R_B - R_A^{obs})}{R_A(R_B - R_A^{obs} + R)}}, \quad [17]$$

and if $R \gg (R_B - R_A)$,

$$R_A \approx \frac{R_A^{obs}}{1 + \dfrac{RM_O^B}{R_A}(R_B - R_A^{obs})}. \quad [18]$$

This equation was already reported by Henkelman *et al.* by integrating Eqs. [1], [2] without saturation of pool B ($\omega_1 = 0$).

MATERIALS AND METHODS

Male Wistar rats (160–220 g body weight) were anesthetized with halothane (0.5% in air). Animals were positioned prone within the magnet, their head placed at the center of the NMR coil (see below). Typically, 120-min anesthesia was required for shimming and to acquire scout views and 90 sets of MT contrast images. Experiments were carried out on a Bruker Biospec 47/50 equipped with a 50-cm horizontal bore, superconducting magnet operating at 4.7 T and additional actively shielded gradients (BGA12, maximum value: 193 mT/m). Measurements were performed with a homemade elliptic Helmholtz resonator (4 cm width, 6 cm length) tuned at 200.3 MHz. Radiofrequency pulses were calibrated for 90° and 180° flip angles using both rectangular and sinc pulses. Proton shimming was made within a 10-mm axial slice localized in the rat brain. Typically, a 30-Hz linewidth at half height was observed for the water proton resonance.

Scout views and MT images were obtained with the RARE sequence (TR = 4000 ms). As thirty-two lines of the *k*-space were acquired within a single shot (TE = 5 ms), four scans were necessary to obtain a 128 × 128 pixels image.

Longitudinal relaxation time T_{1A}^{obs} for brain tissues was measured with an inversion recovery RARE sequence (TR/TE = 6000/5 ms), varying the recovery delay from 20 to 4000 ms.

Transverse relaxation time T_{2A}^{obs} was measured with a T_2-weighted imaging sequence (TR = 3000 ms), varying the echo time from 10 to 200 ms.

T_{1A}^{obs} and T_{2A}^{obs} for various regions of interest (ROIs) were calculated by a least-squares fitting routine (Igor, Wavemetrics, Lake Oswego, OR).

MT images in a single slice were obtained using a continuous wave irradiation prior to the RARE sequence. Partial saturation of the restricted motion proton pool was performed using a continuous wave (CW) excitation at three various ω_1 amplitudes (ω_1 = 660, 1300, and 3000 Hz) and five offset irradiation frequencies (Δ = 750, 1700, 3000, 5700, and 8500 Hz) before turbo spin echo imaging. As mentioned in Table 1, longitudinal relaxation time was about 1 s in the rat brain at 4.7 T for each ROI. Accordingly to this consideration, MT pulse duration (D) was set to 0.3, 0.6, 0.9, 1.2, and 1.5 s to observe the transient decay of the magnetization of pool A. During one experiment carried out on a given animal, images were collected for the whole set of Δ, ω_1, and D values. For each triplet (Δ, ω_1, D), two to four scans were averaged. Signals were collected for three different ROIs: the *corpus callosum* (CC), the basal ganglia (BG), and the temporal lobe (TL). The observed magnetization M_z^A of the liquid pool was normalized to the magnetization M_O^A obtained without off-resonance irradiation, which was measured using 4000 ms repetition time. Due to the

TABLE 1

Relaxation Times and Parameters of the Fit According to the Binary Spin–Bath Model Using a Super-Lorentzian Lineshape for Magnetization Transfer Data in the *Corpus Callosum* (CC), the Basal Ganglia (BG), and the Temporal Lobe (TL) of the Rat Brain ($n = 3$)

	Fitting parameters					Measured relaxation times		
	R (s^{-1})	RM_O^B/R_A	$1/R_AT_{2A}$	T_{2B} (μs)	R_B (s^{-1})	T_{2A}^{obs} (ms)	R_A^{obs} (s^{-1})	R_A (s^{-1})
CC	26 ± 4.5	3.75 ± 0.4	79 ± 12	8.5 ± 0.5	1.41 ± 0.2	53 ± 3	0.83 ± 0.08	0.76 ± 0.08
BG	27.0 ± 4.8	3.58 ± 0.4	81 ± 11	9.35 ± 0.5	1.33 ± 0.14	50.2 ± 3	0.85 ± 0.07	0.80 ± 0.08
TL	34.8 ± 6.3	3.14 ± 0.41	67.3 ± 14	8.3 ± 0.5	1.59 ± 0.24	63 ± 3	0.86 ± 0.07	0.80 ± 0.08

Note. The last column is the result of the calculation according to Eq. [18]. Values are given as mean ± standard deviation.

T_{1A}^{obs} values (Table 1), no correction for incomplete longitudinal recovery was required to calculate M_O^A.

The relative contrast between two ROIs was defined as $|S_i - S_j|$/Noise where i and j represent the different ROIs.

RESULTS

MT imaging experiments were performed on the healthy rat brain *in vivo* at 4.7 T, varying the MT pulse power, duration, and offset-frequency. The fast RARE sequence was employed to produce MT images corresponding to very different acquisition conditions. For the sake of comparison, Fig. 1 shows two typical RARE images (TR/TE = 4000/5 ms), without (Fig. 1A) and with (Fig. 1B) saturation of the restricted pool ($\omega_1 = 660$ Hz and $\Delta = 3000$ Hz, $D = 3$ s) of a rat brain. The relaxation parameter values listed in Table 1 were found to vary weakly according to the brain region. Thus, the image of Fig. 1A could be considered as a proton density image. Conversely, Fig. 1B displays an image in which the contrast is emphasized, due to MT mechanisms. Moreover, the small differences in T_{2A}^{obs} values (see Table 1) were consistent with the poor contrast generally observed with standard T_2-weighted spin echo imaging (not shown) on the rat brain at 4.7 T.

In a previous work (*18*), we derived the five independent parameters R, R_B, RM_O^B/R_A, $1/R_AT_{2A}$, and T_{2B} (reported in Table 1) for several regions of the rat brain under steady-state. Spin echo images were acquired for a number of ω_1 (600–6000 Hz) and Δ (500–20,000 Hz) values. The observed intensities in CC, BG, and TL were modeled according to the last term of Eq. [14], with a Gaussian and a super-Lorentzian lineshape for protons with restricted motions. The latter was found to be more suitable to fit the experimental data. Similar experiments were performed with

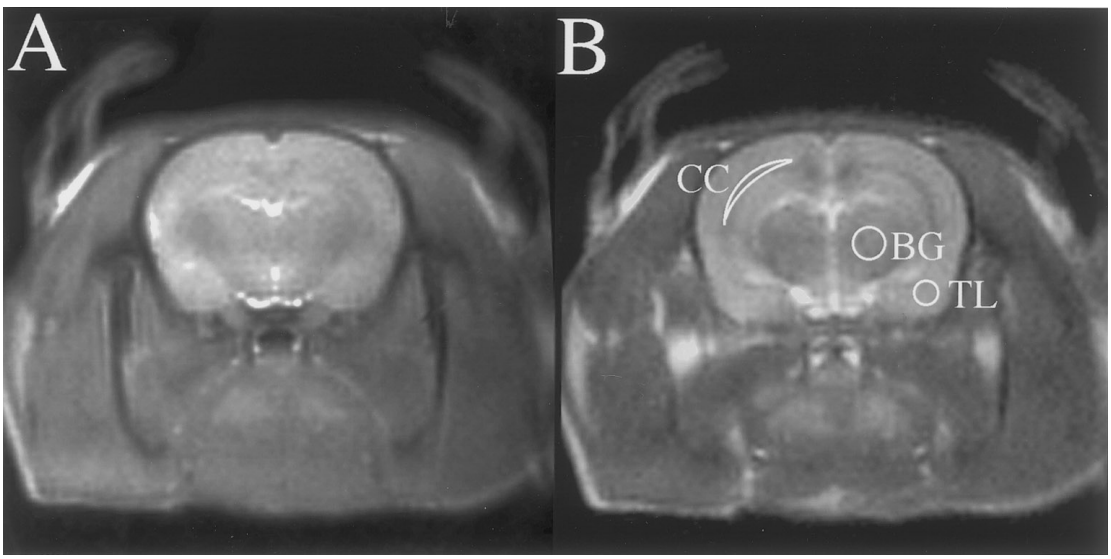

FIG. 1. Axial RARE images from the rat brain *in vivo* at 4.7 T (3 mm slice thickness, 4 cm FOV, matrix size 128 × 128, 4000 ms repetition time, 5 ms echo time, RARE factor 32, 4 accumulations). (A) Proton density image. (B) MT image (off-resonance irradiation power $\omega_1 = 660$ Hz and offset-frequency $\Delta = 3000$ Hz, $D = 3000$ ms). Three considered ROIs are shown: the *corpus callosum* (CC), the basal ganglia (BG), and the temporal lobe (TL).

the RARE sequence on rat brain bearing implanted glioma. The parameters derived from the fits with both techniques were in the same range for CC, BG, and TL and showed the same hierarchy. To shorten experimental time, the RARE sequence was used in the present work to acquire transient decay images. The corresponding fitting parameters are listed in Table 1.

Signal-to-noise ratios acquired from fast imaging experiments were high enough to quantitate MT under several acquisition conditions. Variations of S/N for CC, BG, and TL as a function of Δ, ω_1, and D are presented in Fig. 2. Data were normalized to the S/N ratio measured from the reference image (no MT, see Fig. 1A), to allow comparison between measurement and computer simulation. According to the acquisition parameters, it was possible to decrease S/N from 40 to 1, for each ROI. The observed signal amplitudes displayed in Fig. 2 showed similar behavior for each ROI. As expected, they decreased with lengthening pulse duration, increasing irradiation amplitude, or decreasing Δ.

The longitudinal magnetization decay of pool A could be approximated to be monoexponential provided $|m_2| \gg |m_1.|$ From the relaxation parameters listed in Table 1, m_2/m_1 was calculated for each ROI as a function of the offset-frequency and the irradiation amplitude (Δ and $\omega_1 > 500$ Hz). For all (Δ, ω_1) couples, the ratio was greater than 20.

The $(m_2)^{-1}$ calculated values were in the range of 0.002 to 0.025 s, for (ω_1, Δ), varying from (660 Hz, 500 Hz) to (3000 Hz, 15,000 Hz). Thus, for pulse lengths of 100 ms the second term of Eq. [14] vanishes. Moreover, experimental data obtained for off-resonance pulse lengths ranging from zero to 1.5 s and several combinations (Δ, ω_1) were correctly fitted to a monoexponential decay starting from M_O^A (data not shown). This confirmed that the second term of Eq. [14] could be neglected.

S/N simulations were performed with a super-Lorentzian lineshape for protons with restricted motions (*18*). R_A values presented in Table 1 were derived from the R_A^{obs} ($1/T_{1A}^{obs}$) values measured using the inversion-recovery method according to Eq. [18]. Therefore, R_A values were employed to calculate signal intensities in the transient decay, according to Eq. [16]. Resulting fits were superimposed to experimental data in Fig. 2. Observed and calculated S/N were in good agreement for all the acquisition conditions, which made it possible to simulate signal intensities for each ROI over a wide range of Δ, ω_1, and D.

Relative contrast-to-noise ratio (C/N) between two ROIs were calculated as mentioned above. Contour plots of the results as a function of the offset-frequency and pulse duration are displayed in Fig. 3 for ω_1, giving the optimal C/N value. Maximum contrast values ranged from 3 for BG-CC, 3.1 for BG-TL, and 4.6 for CC-TL (see Figs. 3A, 3B, 3C). Corresponding acquisition conditions were $\omega_1 = 400$ Hz, $\Delta > 10$ kHz, $D > 3$ s for BG-CC; $\omega_1 = 700$ Hz, $\Delta = 2$ kHz, $D = 1.1$ s for BG-TL; and $\omega_1 = 730$ Hz, $\Delta = 5$ kHz, $D \geq 3$ s for TL-CC, respectively. For BG-CC, maximum contrast values vary poorly as a function of the irradiation amplitude, since a contrast-to-noise of 3 was observed without MT pulse.

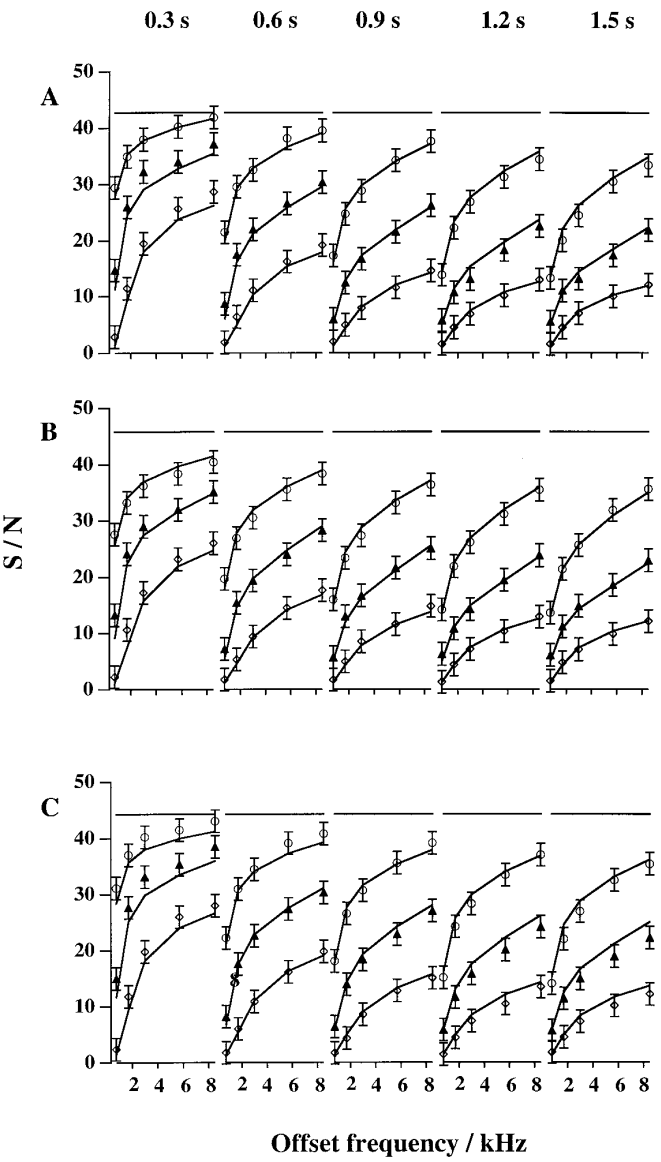

FIG. 2. Signal-to-noise ratios for the CC (A), the BG (B), and the TL (C) as a function of MT pulse offset-frequency. Data are displayed as columns for different MT pulse durations (from 0.3 to 1.5 s) and for ω_1 = 660 Hz (○), 1300 Hz (▲), and 3000 Hz (◇). Error bars indicate the standard deviation. Signal intensities in each ROI were calculated (solid lines) according to Eq. [16] with the fitting parameters listed in Table 1 and normalized to the measured signal-to-noise amplitudes observed without irradiation (horizontal lines).

One should emphasize that calculated optimal C/N could be found for quite different combinations (Δ, D), according to the considered ROI.

Additional imaging experiments were performed under conditions which were chosen to optimize the contrast between BG and TL, and CC and TL. Measured C/N values

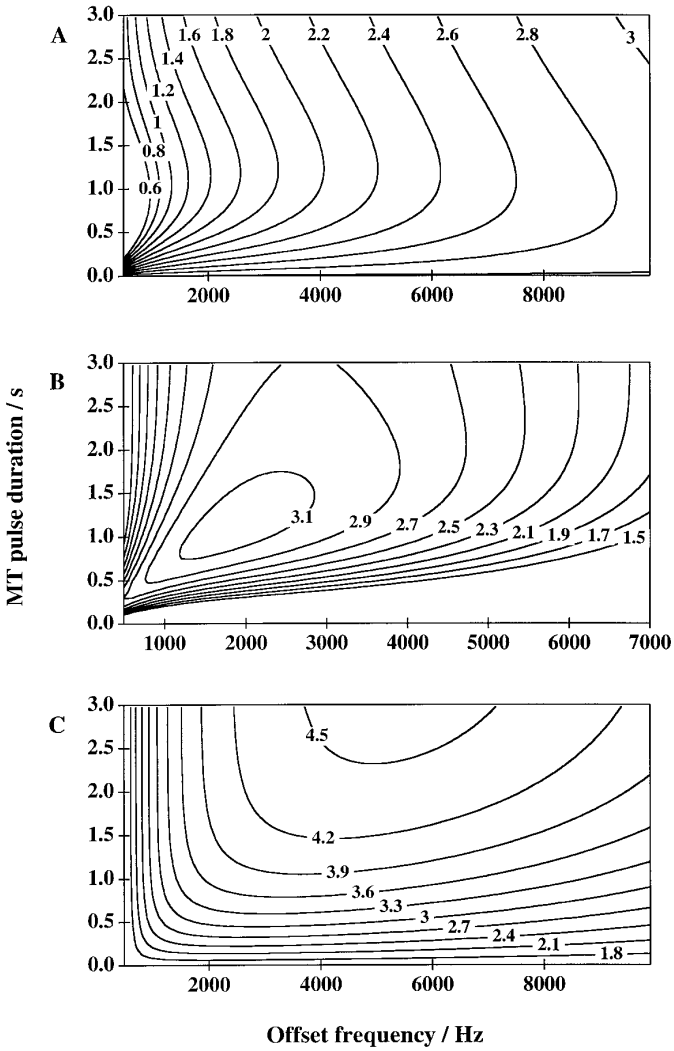

FIG. 3. Contour plots of the calculated comparative contrast-to-noise between BG and CC (A), BG and TL (B), and TL and CC (C) as a function of the offset frequency and irradiation pulse length. ω_1 values are 400 Hz for BG–CC, 700 Hz for BG–TL, and 730 Hz for TL–CC.

were 3.8 ± 0.7 for BG-TL and 4.2 ± 0.8 for CC-TL, in the range of the calculated values (see Figs. 3B and 3C).

DISCUSSION

The present work deals with magnetization transfer *in vivo* on the rat brain at 4.7 T under the non-steady-state condition. A number of previous studies were presented in the literature to describe the MT phenomenon, with radically different approaches. Yeung *et al.* reformulated the spin–bath-model equations by the Redfield–Provotorov theory (*21*), and concluded that a Gaussian lineshape for protons with restricted motions was more suitable than a Lorentzian lineshape. In Ref. (*22*), MT data of cartilage samples were interpreted by a three-component model and a Gaussian lineshape. It seemed clear that these models, including parameters more independent than those of the model used in the present study, could have been successfully applied to the data presented here. Considering the limited accuracy of *in vivo* measurements, we chose to develop a formulation depending on a minimal number of free parameters. With this aim, the two-compartment model (*17*) was generalized to account for the MT signal evolution in the transient decay.

The method proposed here is not fully satisfying from a theoretical point of view, because the super-Lorentzian lineshape is not a solution of the coupled Bloch equations, since a single T_2 rate cannot give rise to anything other than a Lorentzian lineshape. However, the good agreement between observed signal intensities and simulation presented in this study made it possible to consider this model relevant in order to account for MT in the transient decay. This is in agreement with other studies suggesting a super-Lorentzian lineshape for protons with restricted motions. Moreover, more general mathematical expressions for lineshapes of immobilized protons can be introduced in the presented model, such as the Kubo–Tomita lineshape (*25*) or the flexible lineshape recently presented by Li *et al.* (*26*).

The relaxation parameters values listed in Table 1 were derived from fast spin echo experiments. They were in the same range of those obtained from standard spin echo. Nevertheless, the fast imaging RARE sequence reduced experimental time, and two to four images could be accumulated in order to increase the signal-to-noise ratio. Moreover, the use of halothane to anesthetize animals favored the acquisition of a complete data set on the same rat brain. For these reasons, the uncertainties of the fitting parameters were lower than those reported in our previous study (*18*). Therefore, the parameters of Table 1 were chosen to simulate the behavior of longitudinal magnetization of pool A.

One important condition in this study is that the steady-state transverse magnetization has been reached at the end of the MT pulse. For pool B, the T_{2B} values are short enough (see Table 1) to consider $M^{B}_{x,y}$ reached zero after a few milliseconds. On the other hand, $M^{A}_{x,y}$ should reach a near steady-state after several hundreds of milliseconds of MT pulse length. That is why experimental minimal irradiation duration was set to 0.3 s. Fortunately, the optimal contrast values between the selected ROIs were found for pulse duration to be longer than 1.0 s.

This approximation led to simplifications of Bloch equations for longitudinal magnetization of pools A and B, which could be easily integrated. The bi-exponential evolution of M^{A}_{z} (Eq. [14]) was simplified to a monoexponential decay, as long as $m_2/m_1 \gg 1$ and $c_1/c_2 \gg 1$. Experimentally, no bi-exponential decay could be pointed out under various conditions. Moreover, the monoexponential decay of M^{A}_{z} was also observed on agar gel (*17*), on rabbit kidney (*8*), and on the human brain and leg (*27*).

The model presented here was shown to successfully describe signal intensity evolutions for the *corpus callosum*, the basal ganglia, and the temporal lobe, as a function of

TABLE 2
Maximal Calculated Contrast Values between the Implanted C6-glioma and the Other Selected ROIs in the Rat Brain

	$(C/N)_{Max}$	ω_1 (Hz)	Δ (Hz)	D (s)
CC-TUM	12.9	670	4100	2.2
BG-TUM	13.8	730	3000	1.0
TL-TUM	8.7	900	3700	0.8

Note. Experimental conditions leading to these values are given for each ROI couple.

the MT pulse characteristics (Δ, ω_1, and D). The good agreement between simulation and experimental data sets made it possible to predict the observed contrast-to-noise ratios between the selected ROIs. As maximum contrasts between CC–BG, CC–TL, or BG–TL do not correspond to the same acquisition conditions, a prudent compromise should be done, according to the aim sought.

In a previous work, we performed MT images on rat brains with C6-glioma implanted in the basal ganglia (*28*) under steady-state saturation conditions. From these experiments, the relaxation parameters could be derived and according to the model presented here, we calculated the maximum contrast values between the tumor (TUM) and the other ROIs. Maximal contrast-to-noise values and their corresponding acquisition conditions are summarized in Table 2. The D, Δ, and ω_1 values were in the same range as those previously mentioned for BG–CC, BG–TL, and TL–CC. As maximal contrast values between the tumor and the other ROIs were higher than 9, MT imaging is a suitable technique for emphasizing tumor detection in the brain at 4.7 T.

A possible application of the proposed modeling is to anticipate the contrast between white and gray matter in the human brain at 1.0 T from the quantitative analysis of MT recently published by Chai *et al.* (*29*). The authors gave a list of relaxation parameters obtained with on-resonance binomial pulse saturation which could be used for contrast calculation with the model presented here, provided that the proton density in both regions are known. Therefore, we performed experiments on the human brain at 1.5 T with a standard spin echo sequence (TR/TE = 3000/10 ms) without MT. For white matter (WM) and gray matter (GM), signal-to-noise ratios were 44.4 and 50.6 respectively. Taking $[R(s^{-1}), M_O^B, R_B(s^{-1}), R_A\ (s^{-1}), T_{2B}(\mu s), T_{2A}\ (ms)]$ = [21, 0.03, 0.85, 1.05, 12, 73] and [25.5, 0.435, 1.6, 1.9, 10, 91] for GM and WM respectively (see Table 2 of (*28*)), the maximal contrast value was found to be 34 at ω_1 = 6.4 kHz, D = 0.25 s, and Δ = 13.7 kHz. However, the parameter M_O^B reported by Chai *et al.* were given with a rather large uncertainty. In clinical imaging, the SAR for such acquisition conditions *in vivo* on the human brain would be too high. However, a calculated C/N value of about 30 could be obtained, at the same pulse duration, for ω_1 = 1 kHz, Δ = 2 kHz. Other studies should be performed on the human brain to derive relaxation parameters with a better accuracy.

REFERENCES

1. V. Dousset, R. Grossman, K. N. Ramer, M. D. Schnall, L. H. Young, F. Gonzalez-Scarano, E. Lavi, and J. Cohen, Experimental allergic encephalomyelitis and multiple sclerosis: Lesion characterization with magnetization transfer imaging, *Radiology* **182,** 483–491 (1992).
2. A. Gass, G. J. Barker, D. Kidd, J. W. Thorpe, D. MacManus, A. Brennan, P. S. Tofts, A. K. Thompson, W. I. McDonald, and D. H. Miller, Correlation of magnetization transfer ratio with clinical disability in multiple sclerosis, *Ann. Neurol.* **36,** 62–67 (1994).
3. J. W. Thorpe, G. J. Barker, S. J. Jones, I. Moseley, N. Losseff, D. G. MacManus, S. Webb, C. Mortimer, D. L. Plummer, and P. S. Tofts, Magnetization transfer ratios and tranverse magnetization decay curves in optic neuritis: Correlation with clinical findings and electrophisiology, *J. Neurol. Neurosurg. Psychiatry* **59,** 487–492 (1995).
4. F. J. Lexa, R. I. Grossman, and A. C. Rosenquist, MR of wallerian degeneration in the feline visual system: Characterization by magnetization transfer rate with histopathologic correlation, *Am. J. Neuroradiol.* **15,** 201–212 (1994).
5. V. Dousset, B. Brochet, A. Vital, C. Gross, A. Benazzouz, A. Boullerne, A.-M. Bidabe, A.-M. Gin, and J.-M. Caille, Lysolecithin-induced demyelination in primates: Preliminary in vivo study with MR and magnetization transfer, *Am. J. Neuroradiol.* **16,** 225–231 (1995).
6. S. D. Wolff and R. S. Balaban, Magnetization transfer contrast (MTC) and tissue water proton relaxation in vivo, *Magn. Reson. Med.* **10,** 135–144 (1989).
7. J. Grad and R. G. Bryant, Nuclear magnetic cross-relaxation spectroscopy, *J. Magn. Reson.* **90,** 1–8 (1990).
8. J. Eng, T. L. Ceckler, and R. S. Balaban, Quantitative 1H magnetization transfer imaging in vivo, *Magn. Reson. Med.* **17,** 304–314 (1991).
9. N. Lundbom, Determination of magnetization transfer contrast in tissue: An MR imaging study of brain tumor, *Am. J. Roentgenol* **159,** 1279–1285 (1992).
10. H. T. Edzes and E. T. Samulski, Cross-relaxation and spin diffusion in the proton NMR of hydrated collagen, *Nature* **265,** 521–523 (1977).
11. S. Forsen and R. A. Hoffman, Study of moderately rapid chemical exchange reactions by means of nuclear magnetic double resonance, *J. Chem. Phys.* **39,** 2892–2901 (1963).
12. A. R. Gillams, M. S. Silver, and A. P. Carter, Clinical utility of a new contrast option from magnetization transfer contrast, *J. Magn. Reson. Imaging* **5,** 545–550 (1995).
13. M.-G. Jeong, T.-S. Chung, C.-J. Coe, T.-J. Jeon, D.-I. Kim, and A.-Y. Joo, Application of magnetization transfer imaging for intracranial lesions of tuberous sclerosis, *J. Comput. Assist. Tomogr.* **21**(1), 8–14 (1997).
14. N. C. Silver, G. J. Barker, D. G. MacManus, P. S. Tofts and D. H. Miller, Magnetisation transfer ratio of normal brain white matter: A normative database spanning four decades of life, *J. Neurol. Neurosurg. Psychiatry* **62,** 223–228 (1997).
15. G. H. Caines, T. Schleich, and J. M. Rydzewski, Incorporation of magnetization transfer into the formalism for rotating-frame spin–lattice proton NMR relaxation in the presence of an off-resonance-irradiation field, *J. Magn. Reson.* **95,** 558–566 (1991).

16. X. Wu, Lineshape of magnetization transfer via cross relaxation, *J. Magn. Reson.* **94,** 186–190 (1991).

17. R. M. Henkelman, X. Huang, Q. Xiang, G. J. Stanisz, S. D. Swanson, and M. J. Bronskill, Quantitative interpretation of magnetization transfer, *Magn. Reson. Med.* **29,** 759–766 (1993).

18. B. Quesson, E. Thiaudière, C. Delalande, V. Dousset, J.-F. Chateil, and P. Canioni, Magnetization transfer imaging in vivo of the rat brain at 4.7 T: Interpretation using a binary spin–bath Model with a superLorentzian lineshape, *Magn. Reson. Med.,* in press (1997).

19. H. N. Yeung and S. D. Swanson, Transient decay of longitudinal magnetization in heterogeneous spin systems under selective saturation, *J. Magn. Reson.* **99,** 466–479 (1992).

20. R. S. Adler and H. N. Yeung, Transient decay of longitudinal magnetization in heterogeneous spin systems under selective saturation III. Solution by projection operators, *J. Magn. Reson. A* **104,** 321–330 (1993).

21. H. N. Yeung, R. S. Adler, and S. D. Swanson, Transient decay of longitudinal magnetization in heterogeneous spin systems under selective saturation IV. Reformulation of spin–bath-model equations by the Redfield–Provotorov theory, *J. Magn. Reson. A* **106,** 37–45 (1994).

22. R. S. Adler, S. D. Swanson, and H. N. Yeung, A three-component model for magnetization transfer. Solution by projection-operator technique, and application to cartilage, *J. Magn. Reson. B* **110,** 1–8 (1996).

23. J. Listerud, Off-resonance pulsed magnetization transfer in clinical MR imaging: Optimization by analysis of transients, *Magn. Reson. Med.* **37,** 693–705 (1997).

24. C. Morrison, G. J. Stanisz, and R. M. Henkelman, Modeling magnetization transfer for biological-like systems using a semi-solid pool with a super-Lorentzian lineshape and dipolar reservoir, *J. Magn. Reson. B* **108,** 103–113 (1995).

25. R. Kubo and K. Tomita, A general theory of magnetic resonance absorption. *J. Phys. Soc. Jpn.* **9,** 888–919 (1954).

26. J. G. Li, S. J. Graham, and R. M. Henkelman, A flexible magnetization transfer line shape derived from tissue experimental data, *Magn. Reson. Med.* **37,** 866–871 (1997).

27. J. V. Hajnal, C. J. Baudouin, A. Oatridge, I. R. Young, and G. M. Bydder, Design and implementation of magnetization transfer pulse sequences for clinical use, *J. Comput. Assist. Tomogr.* **16,** 17–18 (1992).

28. B. Quesson, A. K. Bouzier, E. Thiaudière, C. Delalande, M. Merle, and P. Canioni, Magnetization transfer fast imaging of implanted glioma in the rat brain at 4.7 T. Interpretation using a binary spin-bath model. *J. Magn. Reson. Imaging* **7,** 1076–1083 (1997).

29. J. W. Chai, C. Chen, J. H. Chen, S. K. Lee, and H. N. Yeung, Estimation of in vivo proton intrinsic and cross-relaxation rates in human brain, *Magn. Reson. Med.* **36,** 147–152 (1996).